

Ferroelectric $Ba_{0.75}Sr_{0.25}TiO_3$ tunable charge transfer in perovskite devices

Zi-Xuan Chen(陈子轩), Jia-Lin Sun(孙家林), Qiang Zhang(张强), Chong-Xin Qian(钱崇鑫), Ming-Zi Wang(王明梓), and Hong-Jian Feng(冯宏剑)

Citation: Chin. Phys. B, 2022, 31 (**5**): 057202. DOI: 10.1088/1674-1056/ac46c3
Journal homepage: http://cpb.iphy.ac.cn; http://iopscience.iop.org/cpb

What follows is a list of articles you may be interested in

Spin depolarization dynamics of WSe_2 bilayer

Binghui Niu(牛秉慧), Jialiang Ye(叶加良), Ting Li(李婷), Ying Li(李莹), Xinhui Zhang(张新惠)
Chin. Phys. B, 2018, 27 (**5**): 057202. DOI: 10.1088/1674-1056/27/5/057202

Effect of CuPc and MoO_3 co-evaporated layer on the conductivity of organic light emitting diodes

He Ze-Shang, Yu Hao-Miao, Peng Huan, Hou Xiao-Yuan
Chin. Phys. B, 2015, 24 (**9**): 097201. DOI: 10.1088/1674-1056/24/9/097201

Electrical bistable devices using composites of zinc sulfide nanoparticles and poly-(N-vinylcarbazole)

Cao Ya-Peng, Hu Yu-Feng, Li Jian-Tao, Ye Hai-Hang, Lü Long-Feng, Ning Yu, Lu Qi-Peng, Tang Ai-Wei, Lou Zhi-Dong, Hou Yan-Bing, Teng Feng
Chin. Phys. B, 2015, 24 (**3**): 037201. DOI: 10.1088/1674-1056/24/3/037201

Ferroelectric $Ba_{0.75}Sr_{0.25}TiO_3$ tunable charge transfer in perovskite devices

Zi-Xuan Chen(陈子轩), Jia-Lin Sun(孙家林), Qiang Zhang(张强), Chong-Xin Qian(钱崇鑫), Ming-Zi Wang(王明梓)†, and Hong-Jian Feng(冯宏剑)‡

School of Physics, Northwest University, Xi'an 710127, *China*

(Received 14 November 2021; revised manuscript received 18 December 2021; accepted manuscript online 29 December 2021)

Interfacial charge recombination is a main issue causing the efficiency loss of the perovskite solar cells (PSCs). Here, ferroelectric $Ba_{0.75}Sr_{0.25}TiO_3$ (BST) is introduced as a polarization tunable layer to promote the interfacial charge transfer of the PSCs. The coexistence of ferroelectric polarization and charge carriers in BST is confirmed by density functional theory (DFT) calculations. Experimental characterization demonstrates the polarization reversal and the existence of domain in BST film. The BST film conductivity is tested as 2.98×10^{-4} S/cm, which is comparable to the TiO_2 being used as the electron transporting layer (ETL) in PSCs. The calculations results prove that BST can be introduced into the PSCs and the interfacial charge transfer can be tuned by ferroelectric polarization. Thus, we fabricated the BST-based PSCs with a champion power conversion efficiency (PCE) of 19.05% after poling.

Keywords: ferroelectric polarization, charge transfer, density-functional theory, perovskite solar cell

PACS: 77.84.–s, 34.70.+e, 31.15.E–, 88.40.hj **DOI:** 10.1088/1674-1056/ac46c3

1. Introduction

Ferroelectrics has been widely investigated by researchers in theory and experiment. The polarization of ferroelectrics can be switched between various directions by exerting different external electric fields.[1] The universal viewpoint believes that the long-range Coulomb interaction induces the displacive ferroelectric polarization but impedes the conductivity.[2] While recent research reveals the correlation between the short-range portion of the Coulomb force and the ferroelectric polarization, in which case the long-range Coulomb force is screened by charge carriers, thus ensures the coexistence of the ferroelectricity and conductivity in bulk ferroelectrics and interfaces.[3–6] Since the development of scanning probe microscopy techniques, domain wall (DW) conductivity in ferroelectrics is experimentally captured even at room temperature, thus triggered series of experimental and theoretical studies on this phenomenon. Commonly, ferroelectric crystals are characterized to have numerous individual domain regions separated by DWs when a ferroelectric phase arose.[7] These localized domain regions spontaneously orient into different directions and form the polarizations. After adding adequate external electric field, the orientations of different domains rotate to rearrange along the field, thus the various domains incorporated and reconfigured into uniform ones.[8–11] During this period, the original domains restructure into new domains.[12,13] Seidel *et al.* investigated the DW conduction behavior in the insulating multiferroic $BiFeO_3$ by means of conductive atomic force microscopy (c-AFM).[14]

Ferroelectrics, especially ferroelectric films, are applied in piezoelectric sensors, microwave electronics, nonvolatile ferroelectric random-access memories, ferroelectric field effect transistors, ferroresistive storage, and multiprobe mass storage.[15–18] Ferroelectrics is a candidate for application in photoelectric devices, such as light emitting diodes, sensors and solar cells, in which the charge transfer can be efficiently tuned with the introducing of ferroelectrics.[19] PSCs have triggered extensive attention since 2009,[20] and its rapid development reveals the considerable application potential.[21–23] $Ba_{1-x}Sr_xTiO_3$ is a traditional dielectric material of which the ferroelectricity can be easily controlled by changing the Sr molar ratio ($x < 0.3$ BST exhibits ferroelectricity at room temperature), which makes it a reliable choice for ferroelectric applications.[24] In a ferroelectrics-based PSC, the built-in-field induced by the ferroelectric polarization will lead to a band realignment of the ferroelectric-photosensitive interface which favours the interfacial charge transfer. Besides, by applying an electric field on the device, the charge transfer direction can also be controlled under the influence of ferroelectric polarization. In addition, the Fermi levels of the selective contacts and the non-radiative recombination in PSCs could both result in a lower open-circuit voltage (V_{oc}). Thus, the BST ferroelectric layer can be introduced into PSCs as both ferroelectric tunable layer and electron transport layer to enhance the built-in-field and suppress the carrier recombination in the trapping states. Moreover, the charge transfer of BST-based devices can be regulated by

†Corresponding author. E-mail: mzwang@nwu.edu.cn
‡Corresponding author. E-mail: hjfeng@nwu.edu.cn

© 2022 Chinese Physical Society and IOP Publishing Ltd

ferroelectric polarization, which is demonstrated by the photovoltaic performance under external poling. In this work, by means of experiments and DFT calculations, we systematically investigate the coexistence of the ferroelectricity and conductivity in BST, as well as the charge transfer of the BST-based devices. Different with the conventional processing of ferroelectric films with high cost, a low temperature chemical solution deposition method is used for BST film fabrication, which effectively reduce the cost of the device. The conductivity of the BST film is 2.98×10^{-4} S/cm, and the champion PCE of the BST-based PSCs is 19.05% after positive poling. The photovoltaic behavior of the BST-based PSCs can be controlled by external poling, which is associated with the tunable charge transfer caused by ferroelectric polarization of BST. Furthermore, the SRIM simulation indicates that the ion implantation is an attemptable method for further device performance improvement.[25]

2. Experimental details

2.1. Materials synthesis

The BST powders are synthesized by a sol–gel method. Firstly, 0.2873 g of barium acetate and 0.0771 g of strontium acetate hemihydrate were mixed with 20 mL of acetic acid, followed by intense stirring at 90 °C until a complete dissolution. The mixture solution was marked as solution 1. Secondly, 0.5125 mL of tetrabutyl titanate and 0.3079 mL of ethylene glycol monomethyl ether were mixed, followed by intense stirring at 50 °C until a complete dissolution. The mixture solution was marked as solution 2. Thirdly, solutions 1 and 2 were mixed, followed by stirring at 50 °C for 2 h. After that, the mixture solution was stored for 24 h in the ambient environment. Lastly, the aged mixture solution was transferred into the muffle furnace for annealing at 850 °C for 20 h, and the final white crystalline powders were grinded for further operation.

The compact-TiO_2 (c-TiO_2) film was fabricated by a chemical deposition method. 200 mL of deionized water was used to create the ice, followed by the dropwise addition of 2.25 mL of titanium tetrachloride at room temperature. After that, the solid–liquid mixture naturally melted into a 0.2-mol/L liquid TiO_2 solution for subsequent deposition. The UV-treated FTO glasses were fixed at the bottom of the culture dish with heat-resistant tapes, and appropriate amount of the TiO_2 solution was added until the liquid level was higher than the FTO substrates. The culture dish was then transferred into the drying oven for a heat treatment at 70 °C for 50 min. The intermediate TiO_2 films were washed alternately by ethyl alcohol and deionized water for 3 times, and dried by N_2 gas fluid. Finally, the intermediate TiO_2 films were annealed at 450 °C for 120 min to crystalize.

The high synthesis temperature of ferroelectric BST will influence the optimal and conductive property of the TiO_2/FTO substrate. To overcome this, a low-temperature chemical deposition similar with that of the c-TiO_2 was employed. For the preparation of the BST solution (see Fig. S1 in supporting-information), appropriate amount of the as-prepared BST powders were added into N, N-dimethylformamide (DMF), followed by stirring at the room temperature for 15 min. After a 3-day standing at the room temperature, the turbid BST solution became transparent with an ideal Tyndall effect. It should be noted that an overlong standing time will cause a poor quality of the fabricated BST film, which leads to a low photovoltaic output of the final device. The process of the BST film deposition (see Fig. S2 in supporting-information) is basically similar with that of the TiO_2 film which is shown in the previous paragraph. To avoid the adverse impact of the residuals on the quality of the BST film, necessary washing and heat-treatment procedure should be carried out, as figure S2 shows. Table S1 shows the information of the materials used for BST preparation and TiO_2/BST-based PSC fabrication.

2.2. Device fabrication

The TiO_2/BST-based PSC was fabricated by the following procedure: The FTO-coated glass was washed in sequence by liquid detergent, acetone, isopropanol, ethyl alcohol, and deionized water, and finally blow-dried by nitrogen gas flow. The FTO substrates were immediately cleaned by ultraviolet ozone for 15 min for the next step. The TiO_2 film was prepared by the chemical deposition method mentioned above. The BST film was prepared as the above method and ultraviolet ozone treated for 15 min before depositing the perovskite layer. For the synthesis of the $FAPbI_3$ precursor, 231.8 mg of FAI, 645.4 mg of PbI_2, and 6.2 mg of $MDACl_2$ were mixed into 1-mL mixture solution of DMF (Alfa, 99.9%) and dimethylsulfoxide (DMSO, Alfa, 99.9%) (8:1, volume ratio) with strong stirring at 25 °C for 3 days in N_2 atmosphere. The $FAPbI_3$ layer was prepared by the deposition method. 50 μL of the $FAPbI_3$ precursor was dropped onto the BST film for spin-coating at 1000 rpm for 10 s and 6000 rpm for 20 s, and 100 μL of the chlorobenzene was dropped at the fifth second from the bottom during the second spinning step. Then the substrates were annealed at 100 °C for 10 min until a dark brown perovskite phase formed. For the deposition of the hole transporting layer (HTL), 90 mg of 2,2′,7,7′-tetrakis(N,N-di-pmethoxyphenylamine)-9,9′-spirobifluorene (spiro-OMeTAD) with 22 μL of the LiTFSI solution (520 mg of LiTFSI in 1 mL of acetonitrile) and 36 μL of 4-tert-butylpyridine (t-BP) were dissolved in 1-mL chlorobenzene, and then spin-coated onto the $FAPbI_3$ film

with 5000 rpm for 30 s. Finally, a 75-nm Au was deposited by thermal evaporation with rate of 1.2 Å/s.

2.3. Characterizations

The x-ray diffraction (XRD) of the BST film was collected by a Bruker D8 Advance power diffractometer with a 6.5-kW Cu $K\alpha$ x-ray radiation (operation at 40 kV and 40 mA). The hysteresis loops were measured on aixACCT TF Analyzer 2000. Transmission electron microscope (TEM) data were acquired from FEI Tecnai G2 F20 microscope. The conductivity was measured by a four-point probe meter (ST-2258C). The steady-state photoluminescence (PL) spectra and the time-resolved PL decay spectra were obtained by a Flex-One Zolix PL instrument. *J*–*V* curves of the TiO_2/BST-based solar cell were obtained from a Keithley 2400 source meter under the illumination of a 100-mW/cm^2 AM 1.5-G condition. The scanning electron microscope (SEM) image was carried out on ZEISS SIGMA scanning electron microscopy.

2.4. Theoretical calculations

The DFT calculation was carried out using Quantum Espresso package.[26,27] The Perdew–Burke–Ernzerhof for solid (PBEsol) functional was applied for exchange correlation interactions.[28] The GBRV ultrasoft pseudopotentials were used for describing the electron–ion interactions.[29] A $2\times2\times2$ *k*-point grid was used, and the plane wave energy cutoff was 400 eV.

The charge displacement curve (CDC) ΔQ between the lowest triplet states and the ground states can be calculated by

$$\Delta Q = \int_{-\infty}^{\infty} \mathrm{d}x \int_{-\infty}^{\infty} \mathrm{d}y \int_{-\infty}^{z} (\rho_{\mathrm{L}} - \rho_{\mathrm{G}})\, \mathrm{d}z, \tag{1}$$

where ρ_{L} and ρ_{G} denote the electron density of the lowest triplet states and the ground states in the real space, respectively.

3. Results and discussion

To investigate the impact of the photo-induced electrons of the photosensitive layer on the ferroelectric polarization of BST, the DFT calculations are used to study the ferroelectric polarization of bulk BST with different electron doping concentration. The electron density increase in bulk BST can be regarded as the consequence of introducing the defect favoring the electrons, such as oxygen vacancy. The electron doping in bulk BST is fulfilled by increasing the amount of the total electrons with a compensation of the positive charges in the background. Figure 1(a) shows the variation of the polarization and the ferroelectric displacement under different electron doping concentrations. For the pure tetragonal BST without electron doping, the DFT calculation gives polarization of 29.50 μC/cm^2, c/a ratio of 1.012, and Ti–O displacement of 0.14 Å. With the increase of the electron doping concentration *n*, the off-center displacement of Ti atom and the ferroelectric polarization decrease for the Coulomb screening effect, as shown in Fig. 1(b). When the electron doping concentration *n* increases to 1.2 *e*/u.c., a sharp decrease of the Ti–O displacement and the ferroelectric polarization will occur, which is attributed by the screening of the long-range Coulomb interaction caused by the electron accumulation. Interestingly, as further increasing of carrier concentration, the Ti–O displacement and the polarization still maintain as *n* reaches a relative high value of 8 *e*/u.c. (0.09 Å and 2.16 μC/cm^2). Experimentally, ion implantation or chemical doping can tune the concentration of Sr. The concentration of Sr can change the concentration of oxygen vacancy in $Ba_{1-x}Sr_xTiO_3$ film, and finally affect electron doping concentration *i.e.*, *n*. These results uncover the coexistence of the ferroelectric phase and the conductivity in bulk BST, indicating the possibility of the electron transfer in bulk ferroelectric BST.

Firstly, we performed the XRD measurement to detect the ferroelectric crystal structure of BST film. In Fig. 2(a), the preferential orientation in $\langle 101 \rangle$ of the as-prepared BST film demonstrates a tetragonal ferroelectric phase with space group *P4mm* (99), and $a = b = 3.977$ Å and $c = 3.988$ Å. The diffraction peaks of the simulated DFT model also matches well with the experiment result. To investigate the polarization response of BST film, we performed the ferroelectric hysteresis (*P*–*E*) loops measurement of BST film. As shown in Fig. 2(b), the saturation polarization is 2.4 μC/cm^2 and the coercive field is 37.3 kV/cm. A four-probe method is utilized to study the conductivity of BST film, and an electric conductivity of 2.98×10^{-4} S/cm is acquired. The conductivity of the as-fabricated BST film is at the same magnitude of the conductivity of TiO_2 film fabricated in the previous work.[30] Additionally, we carried out the TEM measurement to detect the spontaneous ferroelectric polarization of BST film. Figures 2(c)–2(e) show ferroelectric domains in different regions of BST, where the white dashed lines marked with numbers refer to the DWs. The electronic transmission of DWs is discussed in Fig. S3 in supporting information. Figures 2(g) and 2(h) show the fast Fourier transform (FFT) of region I (blue square) and region II (red square) in Fig. 2(f), and figure 2(i) shows the summed FFT of regions I and II. In Fig. 2(i), the evident split of diffraction points demonstrates two ferroelectric domains.[31,32] All these results reveal the spontaneous polarization of the as-fabricated BST film.

Next, to study the charge transfer behavior at the BST/$FAPbI_3$ interface by different ferroelectric polarization, we conducted the charge displacement curve (CDC) and the integrated local density of states (IDOS) calculations. A poling along the direction from $FAPbI_3$ to BST is defined as the

positive poling inducing positive polarization, on the contrary, the negative poling inducing negative polarization. Ti atoms move along the direction perpendicular to the BST/$FAPbI_3$ interface to simulate the ferroelectric polarization under different poling conditions. In Fig. 3(a), as the CDC curves shown, the positive polarization drives the electrons transfer from the $FAPbI_3$ side to the BST side, while the negative polarization contributes to the opposite effect. From the perspective of electronic structure, as shown in Fig. 3(b), the BST/$FAPbI_3$ heterostructure tends to form a type-II band alignment, which proves that the electrons tend to transfer from the $FAPbI_3$ side to the BST side spontaneously. Noteworthily, figure 3(c) shows the band alignment of the BST/$FAPbI_3$ heterostructure under the positive polarization. The band slope facilitates the electron extraction and transfer from $FAPbI_3$ side to BST side. On the contrary, in Fig. 3(d), the negative polarization results in the band slope reversal, impeding electron extraction, and transfer across the BST/$FAPbI_3$ interface. Hence, the BST film as the ETL can effectively tune the charge transfer, and thus improve the photovoltaic performance.

Finally, we experimentally introduce the BST film into the PSC and investigate the ferroelectric polarization effect on interfacial charge transfer and the photovoltaic performance. We firstly investigate the PCE of the TiO_2/BST device with or without positive poling. As shown in Fig. 4(a), the champion PCE of the TiO_2/BST-based solar cell without positive poling (device structure: FTO/TiO_2/BST/$FAPbI_3$/Spiro-OMeTAD/Au) reaches 18.33%, with short-circuit current density (J_{sc}) of 23.34 mA/cm^2, V_{oc} of 1.04 V, and fill factor (*FF*) of 75.54%. The current density–voltage (*J*–*V*) curve of the forward scan shows a PCE of 17.87%, indicating no obvious hysteresis in the TiO_2/BST-based device. For the TiO_2/BST-based solar cell with a +3.7 V/μm positive poling (see next paragraph for discussion about poling), the PCE, V_{oc}, J_{sc}, *FF* all increased. In Fig. 4(b), the cross-sectional SEM image of the TiO_2/BST-based perovskite solar cell is shown. The thickness of TiO_2 film and BST film is 90 nm and 195 nm, respectively.

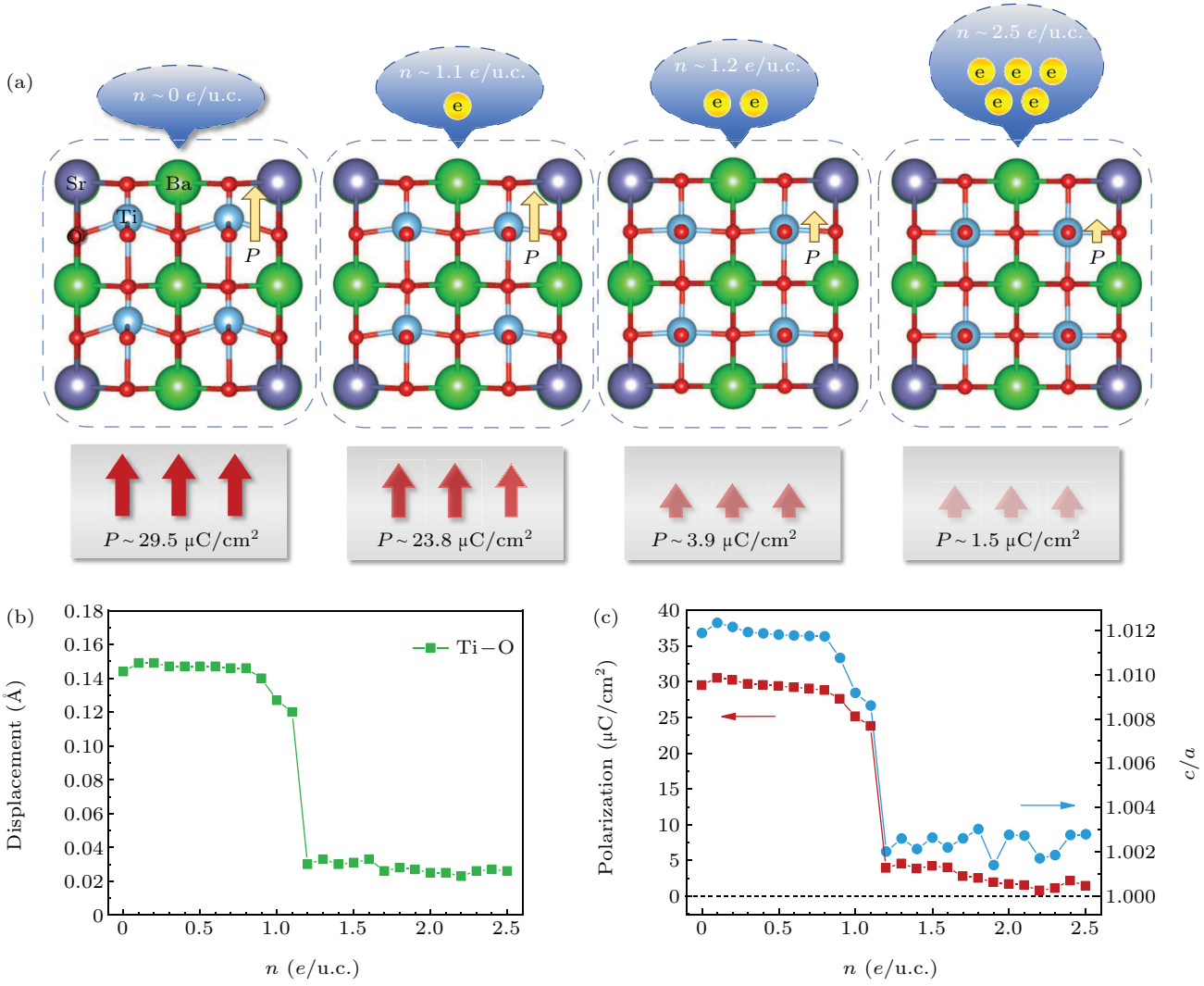


Fig. 1. (a) A schematic diagram describing the existence of the ferroelectric polarization of bulk BST under four typical electron doping situations. (b) Ti–O displacement as a function of the electron doping concentration *n* in bulk BST. (c) The polarization and the ratio of the lattice constants *c* and *a* as a function of the electron doping concentration *n* in bulk BST.

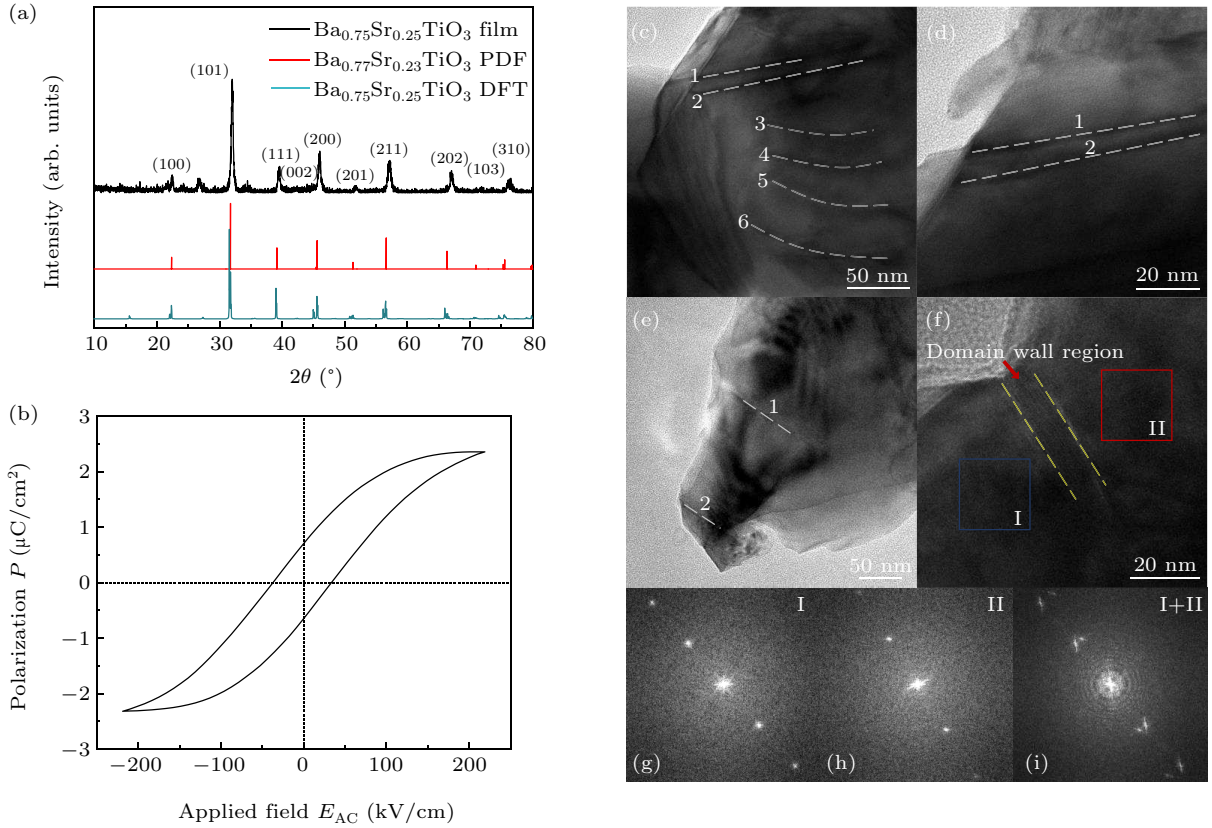


Fig. 2. (a) The XRD of the experimentally fabricated $Ba_{0.75}Sr_{0.25}TiO_3$ film, $Ba_{0.77}Sr_{0.23}TiO_3$ standard PDF card, and the DFT calculation model. (b) The *P*–*E* loops of the BST film. (c)–(f) The TEM images of the BST film with domains and DWs indicated by white dashed lines. (g)–(i) FFTs of blue and red region in panel (f), and their summed one.

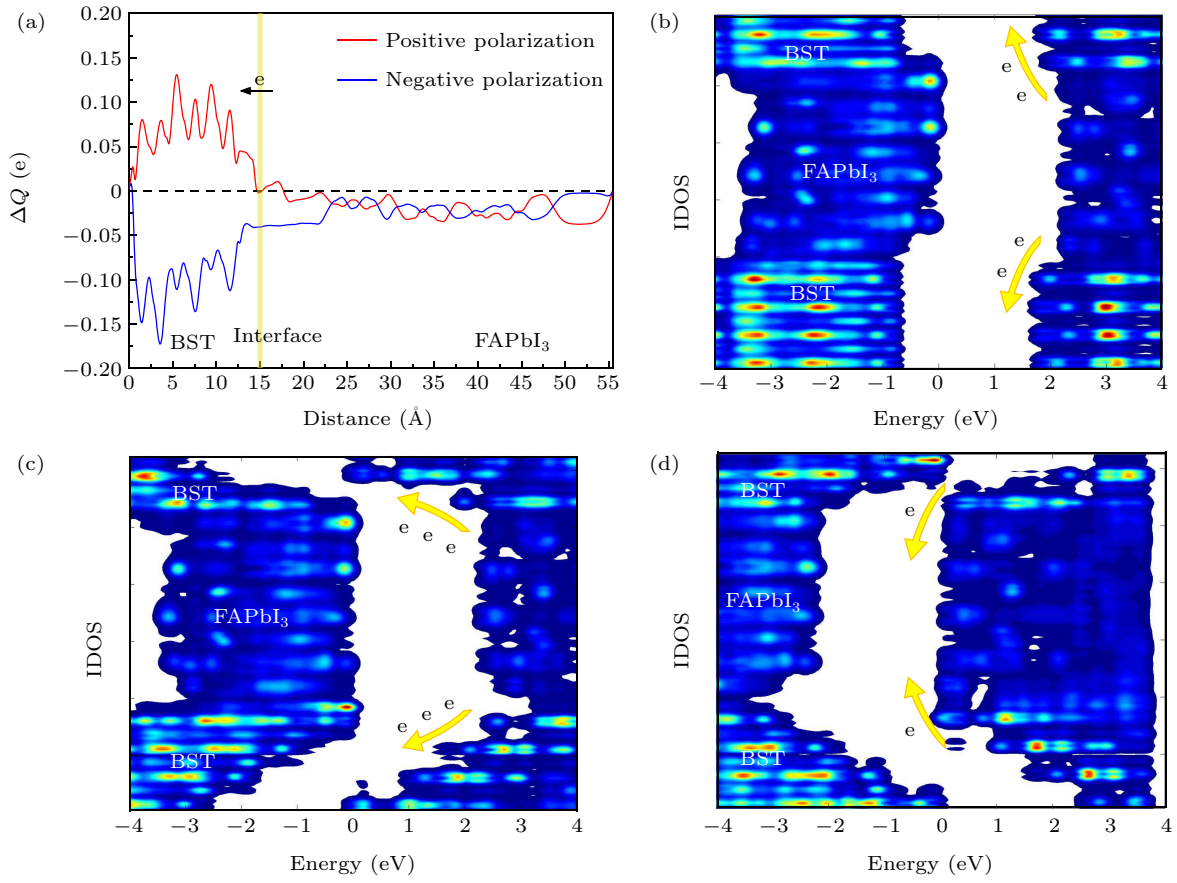


Fig. 3. (a) The CDC of BST/$FAPbI_3$ heterostructure under different poling conditions. The IDOS projected along the ⟨001⟩ direction of BST/$FAPbI_3$ heterostructure with (b) no polarization, (c) positive polarization, and (d) negative polarization.

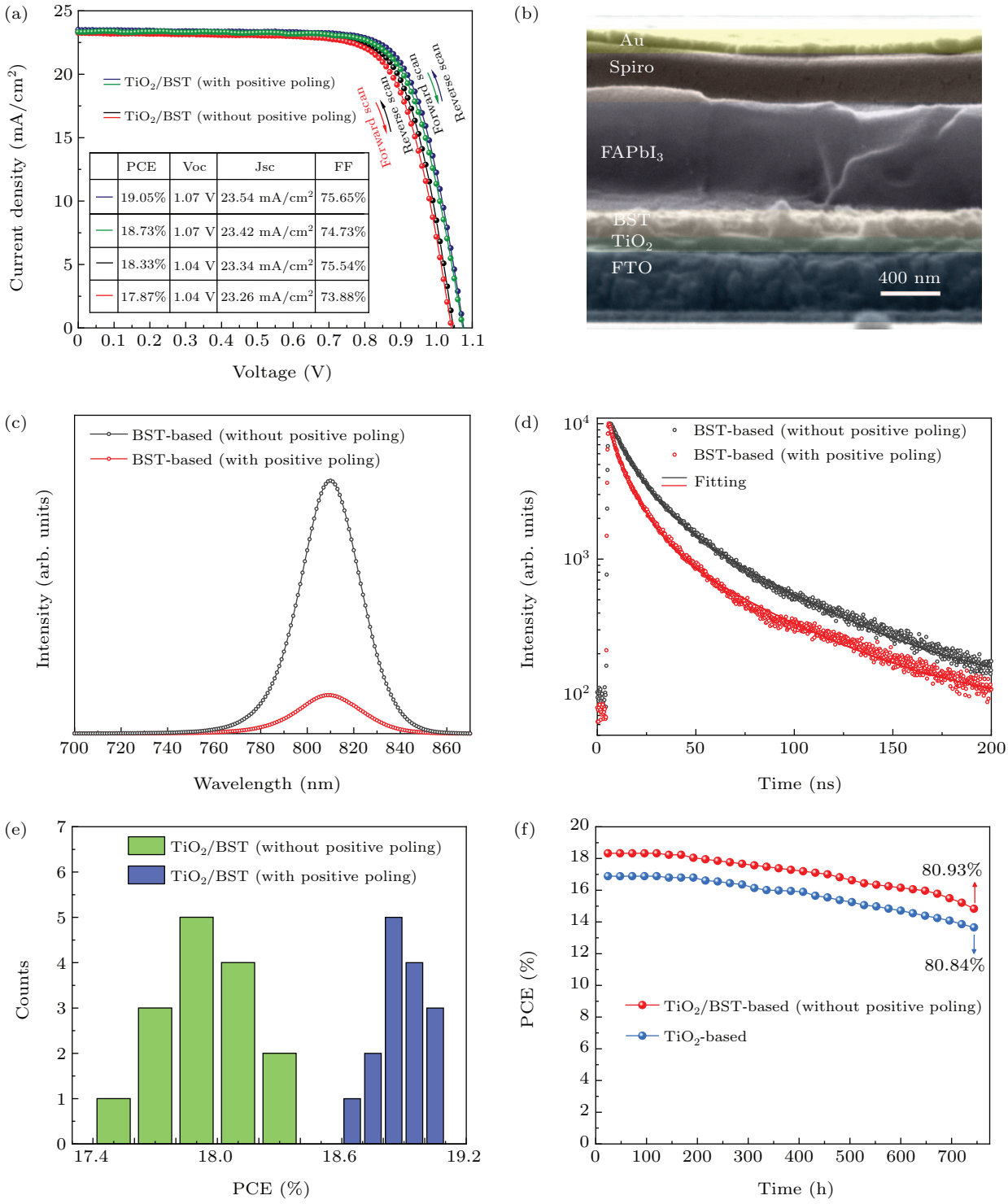


Fig. 4. (a) The *J*–*V* curves (under reverse and forward scan) of the champion PCE of TiO_2/BST-based PSC with and without positive poling. (b) The cross-sectional SEM image of the TiO_2/BST-based solar cell. (c) The steady-state PL spectra and (d) the time-resolved PL decay spectra of the BST-based film (FTO/TiO_2/BST/$FAPbI_3$/Spiro) with or without positive poling. (e) The statistics PCE diagram of 15 TiO_2/BST-based devices with and without positive poling. (f) The diagram of the stability measurement of unencapsulated TiO_2/BST-based and TiO_2-based devices in atmosphere environment with $45 \pm 5\%$ humidity and room temperature for over 750 hours.

The steady-state PL and time-resolved PL decay were carried out to investigate the influence of ferroelectric polarization on charge transfer dynamics. Figure 4(c) shows the steady-state PL spectra of the BST-based film (FTO/TiO_2/BST/$FAPbI_3$/Spiro) with or without positive poling. According to the coercive field (37.3 kV/cm) of the BST film (Fig. 2(b)), we applied a positive poling (+3.7 V/μm) on the FTO/TiO_2/BST film for 30 min to change the spontaneous polarization of BST into a positive polarization which is more favorable to electron extraction from $FAPbI_3$ layer to BST layer. As a result, the BST-based film with positive poling shows an obvious PL intensity decrease, indicating an enhanced electron transfer from $FAPbI_3$ layer to BST layer. In Fig. 4(d), the time-resolved PL decay is also in agreement

with the steady-state PL. The PL decay lifetime of the BST-based films without and with positive poling are 35 ns and 29 ns, respectively. The PL quenching of the BST-based film with positive poling is faster than the BST-based film without positive poling. The shortened PL lifetime of the BST-based film with positive poling suggests an enhanced electron transfer from $FAPbI_3$ layer to BST layer. These results experimentally demonstrate that the ferroelectric polarization can tune the electron transfer between the BST/$FAPbI_3$ interface.

Figure 4(e) shows the statistics PCE diagram of 15 TiO_2/BST-based devices with and without positive poling. The average PCE increased from 17.97% to 18.89% after adding a +3.7-V/μm positive poling. After optimizing the fabrication of $FAPbI_3$ film, the stability of $FAPbI_3$ film increased and the corresponding $FAPbI_3$-based device efficiency maintains 80% of the original one after 30 days (Fig. 4(f)). An unencapsulated TiO_2/BST-based and TiO_2-based device with initial PCE of 18.33% and 16.89% are stored in atmosphere environment with $45 \pm 5\%$ humidity and room temperature. The device photovoltaic performance comparison about TiO_2-based, TiO_2/BST-based (with and without positive poling) solar cells is discussed in Fig. S4 in supporting-information.

4. Conclusions

In conclusion, we theoretically investigate the varying Ti off-center displacement, *c*/*a* ratio and polarization of BST under different electron doping concentration. Coexistence of the conductivity and the ferroelectricity is found in BST. The TEM results demonstrate the ferroelectric domains in BST. The CDC and the IDOS further prove the tunable interfacial charge transfer. We introduce the ferroelectric BST film into the TiO_2-based PSCs and acquire the PCE of 18.33% without positive poling, and a positive poling will increase the PCE to 19.05%. The interfacial charge transfer and the photovoltaic performance of the TiO_2/BST/$FAPbI_3$-based PSCs can be tuned by poling. The PL results demonstrate the tunable charge transfer across the BST/$FAPbI_3$ interface. The coexistence of ferroelectricity and conductivity in ferroelectric BST broadens the application of lead-free ferroelectric BST in perovskite optoelectronic devices.

Acknowledgments

Project supported by the National Natural Science Foundation of China (Grant Nos. 51972266, 51672214, and 11904286) and the Natural Science Basic Research Program of Shaanxi Province, China (Grant No. 2022JZ-01).

References

[1] Lines M E and Glass A M 1977 *Principles and Applications of Ferroelectrics and Related Materials* (Oxford: Oxford University Press) pp. 102–103
[2] Wurfel P and Batra I P 1973 *Phys. Rev. B* **8** 5126
[3] Wang Y, Liu X H, Burton J D, Jaswal S S and Tsymbal E Y 2012 *Phys. Rev. Lett.* **109** 247601
[4] Sharma P, Xiang F X, Shao D F, Zhang D W, Tsymbal E Y, Hamilton A R and Seidel J 2019 *Sci. Adv.* **5** eaax5080
[5] Liu X H, Tsymbal E Y and Rabe K M 2018 *Phys. Rev. B* **97** 094107
[6] Zhang Y, Lu H D, Xie L, Yan X X, Paudel T R, Kim J, Cheng X X, Wang H, Heikes C, Li L Z, Xu M J, Schlom D G, Chen L Q, Wu R Q, Tsymbal E Y, Gruverman A and Pan X Q 2018 *Nat. Nanotechnol.* **13** 1132
[7] Chen G Z, Jin L, Min T and Xiao J 2021 *Chin. Phys. Lett.* **38** 087701
[8] Leo N, Carolus V, White J S, Kenzelmann M, Hudl M, Toédano P, Honda T, Kimura T, Ivanov S A, Weil M, Lottermoser Th, Meier D and Fiebig M 2018 *Nature* **560** 466
[9] Nahas Y, Prokhorenko S, Fischer J, Xu B, Carrétéro C, Prosandeev S, Bibes M, Fusil S, Dkhil B, Garcia V and Bellaiche L 2020 *Nature* **577** 47
[10] Nelson C T, Gao P, Jokisaari J R, Heikes C, Adamo C, Melville A, Baek S H, Folkman C M, Winchester B, Gu Y J, Liu Y M, Zhang K, Wang E, Li J Y, Chen L Q, Eom C B, Schlom D G and Pan X Q 2011 *Science* **334** 968
[11] You L, Zheng F, Fang L, Zhou Y, Tan L Z, Zhang Z Y, Ma G H, Schmidt D, Rusydi A, Wang L, Chang L, Rappe A M and Wang J L 2018 *Sci. Adv.* **4** eaat3438
[12] Sharma P, Zhang Q, Sando D, Lei C H, Liu Y Y, Li J Y, Nagarajan V and Seidel J 2017 *Sci. Adv.* **3** e1700512
[13] Li Z W, Wang Y J, Tian G, Li P L, Zhao L N, Zhang F Y, Yao J X, Fan H, Song X, Chen D Y, Fan Z, Qin M H, Zeng M, Zhang Z, Lu X B, Hu S J, Lei C H, Zhu Q F, Li J Y, Gao X S and Liu J M 2017 *Sci. Adv.* **3** e1700919
[14] Seidel J, Martin L W, He Q, Zhan Q, Chu Y H, Rother A, Hawkridge M E, Maksymovych P, Yu P, Gajek M, Balke N, Kalinin S V, Gemming S, Wang F, Catalan G, Scott J F, Spaldin N A, Orenstein J and Ramesh R 2009 *Nat. Mater.* **8** 229
[15] Scott J F 2007 *Science* **315** 954
[16] Setter N, Damjanovic D, Eng L, Fox G, Gevorgian S, Hong S, Kingon A, Kohlstedt H, Park N Y, Stephenson G B, Stolitchnov I, Taganstev A K, Taylor D V, Yamada T and Streiffer S 2006 *J. Appl. Phys.* **100** 051606
[17] Martin L W and Rappe A M 2016 *Nat. Rev. Mater.* **2** 16087
[18] Zhao Y P, Wang C, Zheng X F, Ma X H, Li A, Liu K, He Y L, Lu X L and Hao Y 2021 *Chin. Phys. B* **30** 057302
[19] Li Z Z, Tang R S, Wang X F and Zheng F G 2014 *Chin. Phys. Lett.* **31** 047701
[20] Kojima A, Teshima K, Shirai Y and Miyasaka T 2009 *J. Am. Chem. Soc.* **131** 6050
[21] Li M, Yang Y G, Wang Z K, Kang T, Wang Q, Turren-Cruz S H, Gao X Y, Hsu C S, Liao L S and Abate A 2018 *Adv. Mater.* **30** 1800258
[22] Zhang Z Y, Xu L and Qi J J 2021 *Chin. Phys. B* **30** 038801
[23] Liu Y H, Wang W, Xiao F, Xiong L B and Ming X 2021 *Chin. Phys. B* **30** 108102
[24] Cheng J G, Meng X J, Li B, Tang J, Guo S L, Chu J H, Wang M, Wang H and Wang Z 1999 *Appl. Phys. Lett.* **75** 2132
[25] Stoller R E, Toloczko M B, Was G S, Certain A G, Dwaraknath S and Garner F A 2013 *Nucl. Instrum. Methods Phys. Res. B* **310** 75
[26] Giannozzi P, Baroni S, Bonini N, *et al.* 2009 *J. Phys.: Condens. Matter.* **21** 395502
[27] Walker B, Saitta A M, Gebauer R and Baroni S 2006 *Phys. Rev. Lett.* **96** 113001
[28] Perdew J P, Ruzsinszky A, Csonka G I, Vydrov O A, Scuseria G E, Constantin L A, Zhou X L and Burke K 2008 *Phys. Rev. Lett.* **100** 136406
[29] Garrity K F, Bennett J W, Rabe K M and Vanderbilt D 2014 *Comput. Mater. Sci.* **81** 446
[30] Wojciechowski K, Saliba M, Leijtens T, Abate A and Snaith H J 2014 *Energy Environ. Sci.* **7** 1142
[31] Sæterli R, Rørvik P M, You C C, Holmestad R, Tybell T, Grande T, van Helvoort A T J and Einarsrud M A 2010 *J. Appl. Phys.* **108** 124320
[32] Fu M S, Ni L, Liu X Q, Chen X M and Zeng Y W 2012 *J. Am. Ceram. Soc.* **95** 2979